Electrical Characterization of Basal Cell Carcinoma Using a Handheld Electrical Impedance Dermography Device

Xuesong Luo[1], Ye Zhou[1], Tristan Smart[2], Douglas Grossman[2,3] and Benjamin Sanchez[1]

Sensitive, objective, and easily applied methods for evaluating skin lesions are needed to improve diagnostic accuracy. In this study, we evaluated whether a developed noninvasive electrical impedance dermography device URSKIN could serve this purpose. In this pilot study, 17 subjects with subsequently confirmed basal cell carcinoma underwent four-electrode electrical impedance dermography measurements to assess the electrical properties of basal cell carcinoma and adjacent normal skin. A linear mixed-effects model with random intercept and slope terms was used for the analysis of multifrequency values in longitudinal and transverse directions. A significant difference in the intercept of frequency trajectories was observed for the longitudinal conductivity of 0.13 siemens/m ($P < 0.001$, 95% confidence interval = 0.10−0.16), transverse conductivity of 0.06 siemens/m ($P < 0.001$, 95% confidence interval = 0.05−0.07), longitudinal relative permittivity (dimensionless) of 203,742 ($P < 0.001$, 95% confidence interval = 180,292−227,191), and transverse relative permittivity (dimensionless) of 86,894 ($P < 0.001$, 95% confidence interval = 81,549 − 92,238). Thus, our device detected significant electrical differences between basal cell carcinoma and adjacent normal skin. Given these preliminary performance metrics and the ease of use, this technology merits further study to establish its value in facilitating the clinical diagnosis of skin cancers.

JID Innovations (2022);**2:**100075 doi:10.1016/j.xjidi.2021.100075

INTRODUCTION

Although many skin cancers are easily recognized by the naked eye, they can be difficult to diagnose at early stages, and therefore, there is a need and opportunity to develop technologies that can facilitate clinical diagnosis (March et al., 2015). Nonvisual electrical impedance dermography (EID), a term coined by the authors to refer to the specific application of impedance techniques for skin cancer assessment, is a technology based on the detection of volume conduction differences between benign and malignant skin tissue (Braun et al., 2017; Rocha et al., 2017). These volume conduction properties (VCPs) reflect (i) how strongly skin resists or conducts alternating electrical current and (ii) its capacity to store electrical (positive and negative) ions charged inside and outside the cells. VCPs are uniquely determined by two physical electrical quantities: conductivity in the International System of units of siemens/m and relative permittivity (this is a dimensionless quantity because it is defined with respect to the permittivity of vacuum) (Foster and Schwan, 1989). VCPs are characteristic physical properties (in the same way as the density, color, hardness, melting, or boiling points) and represent an objective measure that describes the electrical status of the skin on a universally standard and absolute scale (Sanchez et al., 2021). Alterations in the internal composition and structure of cancerous skin tissue will result in an imbalance of the ionic content and cellular integrity, which will affect its VCPs.

To detect pathological changes inducing alterations in VCPs for skin diagnostic purposes, EID typically applies a low-intensity electrical alternating current to the tissue in a given area using two electrodes. As current flows through tissue, it generates a voltage signal that is then measured using the same (or different) electrodes. The voltage-to-current relationship determines the apparent electrical impedance of the skin (Stephens, 1963), a quantity measured that arises from the interaction of the skin conductivity and relative permittivity properties as well as their dependence with the frequency of electrical current and direction of application (Yamamoto and Yamamoto, 1976). Then, VCPs of skin can be inferred from impedance values using a biophysical model that describes the measurement configuration and the propagation of the electrical current within the skin.

Unlike the VCPs that are intrinsic characteristics of the skin, electrical impedance does not provide standardized values because they are also dependent on the electrode configuration (Geddes, 1996). That is, simply by modifying the distance between the current and/or the voltage

[1]*Department of Electrical & Computer Engineering, University of Utah, Salt Lake City, Utah, USA;* [2]*Huntsman Cancer Institute, University of Utah Health Sciences Center, Salt Lake City, Utah, USA; and* [3]*Department of Dermatology, University of Utah Health Sciences Center, Salt Lake City, Utah, USA*

Correspondence: Benjamin Sanchez, Department of Electrical & Computer Engineering, University of Utah, Sorenson Molecular Biotechnology Building, 36 South Wasatch Drive, Office 3721, Salt Lake City, Utah 84112, USA. E-mail: benjamin.sanchez@utah.edu

Abbreviations: BCC, basal cell carcinoma; EID, electrical impedance dermography; ICC, intraclass correlation coefficient; VCP, volume conduction property

Received 12 August 2021; revised 1 November 2021; accepted 2 November 2021; accepted manuscript published online XXX; corrected proof published online XXX

Cite this article as: JID Innovations 2022;2:100075

Table 1. Subject Demographics and Clinicopathologic Features of Lesions

Subject #	Age	Sex (M, F)	Body Site	Lesion Size (mm)	Diagnosis	BCC Subtype
1	63	M	Shoulder	5	BCC	Superficial
2	73	M	Shoulder	5	BCC	Superficial
3	91	F	Arm	10	BCC	Superficial, focally Infiltrative
4	36	F	Forearm	5	BCC	Superficial, micronodular
5	74	M	Clavicle	6	BCC	Superficial, nodular
6	76	F	Forearm	6	BCC	Superficial
7	59	M	Back	5	BCC	Superficial, nodular
8	52	M	Back	5	BCC	Superficial
9	44	M	Scalp	7	BCC	Superficial, nodular
10	54	M	Back	7	BCC	Superficial
11	58	M	Shoulder	7	BCC	Superficial
12 (excluded)	49	F	Hand	5	Telangiectasia	NA
13	55	M	Back	11	BCC	Superficial
14	73	F	Arm	6	BCC	Superficial
15	60	M	Neck	7	BCC	Superficial
16	48	F	Back	9	BCC	Superficial
17	35	F	Shoulder	6	BCC	Micronodular, infiltrative
18	61	F	Shin	6	BCC	Superficial

Abbreviations: BCC, basal cell carcinoma; F, female; M, male; NA, not applicable.

electrodes, the impedance values will be different even if the skin is exactly the same. Furthermore, depending on the number of electrodes used to measure the skin, the impedance values will contain as well the contribution of the skin–electrode polarization impedance (McAdams et al., 1995; Schwan, 1992) as it is the case for the Nevisense two- and three-electrode device (SciBase, Stockholm, Sweden). The skin–electrode polarization impedance arises from the interface between the electrode (a metallic conductor where the current charge carriers are electrons) and the skin (where the electrical current conduction consists of the transit of ions, i.e., atoms of positive or negative charge). Importantly, the skin–electrode polarization impedance is a poorly controllable experimental factor where small alterations in skin–electrode contact area, skin humidity, or temperature can give large impedance variations between measurements, especially at low frequency (Alonso et al., 2020). Although research has confirmed the diagnostic value of this approach (Glickman et al., 2003; Malvehy et al., 2014), it still remains unknown to what extent impedance differences detected in those studies were solely generated by changes in the underlying VCPs in cancerous skin tissues and not a secondary interface effect between skin and the electrodes.

In this study, we performed a pilot study testing a prototype of a four-electrode EID device named URSKIN developed at the University of Utah (Salt Lake City, UT) for measuring in situ skin VCPs as well as their directionality. We determined the intrasession reproducibility of the technique and assessed skin electrical differences between basal cell carcinoma (BCC) and adjacent normal skin.

RESULTS

Subject recruitment and lesion characteristics

A total of 18 subjects with skin lesions clinically suspicious for BCC were recruited for the study. Subject demographics and clinicopathologic characteristics of the lesions are detailed in Table 1. Given the intended use of the device for early detection of skin cancers, we targeted enrollment to early-stage lesions that were primarily macular and avoided larger palpable or ulcerated lesions. All lesions were assessed by a dermatologist (DG). After EID measurements using URSKIN (Figure 1), all lesions were biopsied, and 17 of 18 were confirmed to be BCC. A total of 11 lesions exclusively revealed a superficial histologic pattern; 5 lesions revealed a combination of superficial, nodular, micronodular, and focally infiltrative patterns; and 1 lesion revealed a combination of micronodular and infiltrative patterns. One lesion (subject 12) revealed only telangiectasia and was excluded from the analyses.

Device usability and reproducibility

A minimum of three impedance measurements at six different frequencies of electrical current ranging from 8 to 256 kHz was taken from lesional and adjacent clinically normal skin. The time required for data collection was <5 minutes per subject. Test–retest reproducibility data are summarized in Table 2. For both the lesional and normal skin measurements, intraclass correlation coefficient (ICC) conductivity values were lower at 8 and 16 kHz with mean values that ranged from 0.245 to 0.63. Comparatively, relative permittivity ICC values showed better reproducibility at 16 kHz with mean estimates from 0.673 to 0.822, where an ICC value of 1 represents a perfectly reproducible test. We found the most reproducible frequency range with the highest ICC to be 128 kHz, with mean estimates ranging from 0.61 to 0.913 except for longitudinal relative permittivity that was 32 kHz with ICC values of 0.814 and 0.883 for lesional and normal skin, respectively.

Electrical differences between BCC and normal skin

Multifrequency VCPs data, including subject-repeated measurements, were analyzed and modeled with a mixed-effect linear model with random intercept and slope for BCC and

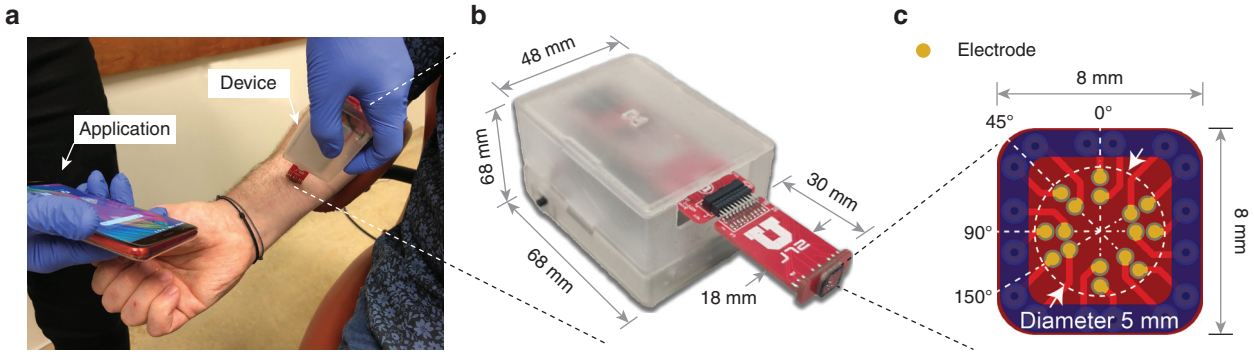

Figure 1. Handheld EID device tested in this study. (**a**) Use of example in the clinic. (**b**) The reduced dimensions and portability of URSKIN allow the operator to hold the device with one hand, whereas the other hand controls the device with a smartphone (please see the Supplementary Materials and Methods for additional details). (**c**) The electrode spacing used in this study constrains the minimum lesion size to 5 mm. EID, electrical impedance dermography.

normal skin, and the data are shown in Figures 2 and 3. Modeling a random slope gave lower Akaike scores than a random intercept model only both for conductivity and relative permittivity in longitudinal and transverse directions. We intentionally did not model the interaction between group and frequency because there is no physiological rationale supporting this dependence. For this, we included the slope in our linear-effect model, which models the Maxwell–Wagner frequency–dependent relaxation due to cellular membrane permeability in the frequency range measured (Schwan, 1984). As expected from the Maxwell–Wagner interfacial polarization mechanism in biological tissues, the slopes of both BCC and normal skin conductivity curves increase with frequency, whereas the frequency dependence of relative permittivity curves is opposite. Modeling results, summarized in Table 3, reveal significant intercept differences ($P < 0.001$) between BCC and normal skin. These intercept differences are physiologically interpretable because they represent the VCPs of skin extrapolated at 0 Hz where the electric current flows only through the extracellular medium owing to the capacitive behavior of cellular membranes. These results suggest that the intercept is a sensitive model parameter to detect extracellular compositional and structural differences in BCC and adjacent nonlesional skin tissue.

DISCUSSION

The goal of this study was to evaluate the feasibility of our technology to measure the VCPs of BCC, the most common form of skin cancer. Thus, we focused our initial efforts on determining the reproducibility of the technique in a clinical setting and the modeling differences between BCC and normal skin. The URSKIN device yielded highly reproducible measurements that revealed significant electrical differences between BCC and normal skin. In addition, we found our device easy to use, and data collection was quick and painless for the subjects.

To assess the reproducibility, we performed repeated measurements with our electrode array placed over the skin lesion on the basis of visual inspection. This somewhat imprecise approach to electrode placement may be offset to some extent by the fact that the array provides electrodes that are entirely fixed in position relative to one another, thus reducing intra-array differences in electrode spacing or

Table 2. Summary of Test Versus Retest Reproducibility for Multifrequency Conductivity and Relative Permittivity Values

		Longitudinal Conductivity		Transverse Conductivity		Longitudinal Relative Permittivity		Transverse Relative Permittivity	
Frequency (kHz)		Estimates	CI (95%)	Estimates	CI (95%)	Estimates	CI (95%)	Estimates	CI (95%)
8	BCC	0.334	0.034–0.65	0.445	0.146–0.72	0.379	0.087–0.673	0.548	0.227–0.76
	Normal	0.245	−0.053 to 0.586	0.3	0.011–0.622	0.595	0.308–0.816	0.494	0.203–0.755
16	BCC	0.384	0.079–0.686	0.63	0.352–0.835	0.731	0.502–0.885	0.739	0.435–0.889
	Normal	0.258	−0.059 to 0.611	0.478	0.173–0.753	0.673	0.405–0.862	0.822	0.64–0.93
32	BCC	0.545	0.234–0.801	0.0569	−0.23 to 0.457	0.814	0.615–0.9	0.645	0.257–0.858
	Normal	0.247	−0.038 to 0.589	0.709	0.462–0.878	0.883	0.745–0.955	0.869	0.726–0.949
64	BCC	0.775	0.562–0.909	0.776	0.563–0.91	0.713	0.467–0.88	0.481	0.107–0.742
	Normal	0.58	0.272–0.821	0.62	0.323–0.841	0.275	−0.028 to 0.625	0.704	0.432–0.882
128	BCC	0.715	0.122–0.715	0.832	0.667–0.931	0.00571	−0.236 to 0.347	0.728	0.44–0.88
	Normal	0.843	0.683–0.936	0.61	0.328–0.824	0.449	0.147–0.729	0.913	0.816–0.966
256	BCC	0.535	0.238–0.787	0.822	0.631–0.93	0.225	−0.072 to 0.579	0.656	0.264–0.861
	Normal	0.29	−0.006 to 0.624	0.523	0.213–0.782	0.111	−0.18 to 0.491	0.605	0.317–0.826

Abbreviations: BCC, basal cell carcinoma; CI, confidence interval.
Estimates of intraclass correlation coefficients and 95% Cis are shown.

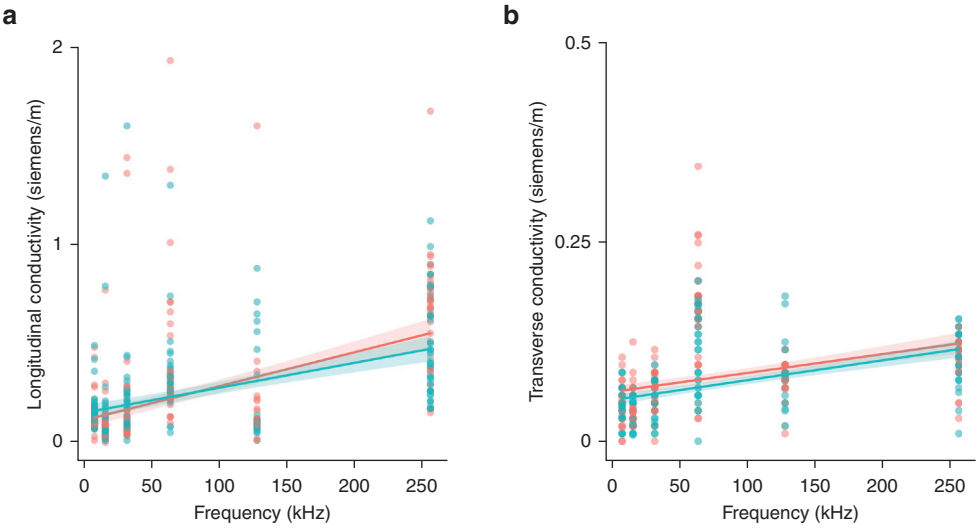

Figure 2. Conductivity of BCC and normal adjacent skin. BCC (red) and nonlesional adjacent skin (blue) dots represent individual conductivity values obtained in (**a**) longitudinal and (**b**) transverse directions, including all repeated measurements and subjects. The solid lines are the modeled trajectories, including 95% confidence intervals. BCC, basal cell carcinoma.

orientation. Thus, the reproducibility of the electrode placement could be further improved by marking the skin with a marker or a pinpoint tattoo to assist in accurate placement during repeated measurements. Other potential sources of error affecting the reproducibility of the technique include the variability in the amount of saline used to moisten the skin before the measurements, the time to measurement after applying saline, as well as the pressure applied to hold the electrode in place over the skin. Despite these potential confounding variables, the test–retest reproducibility was high at intermediate frequencies, suggesting that these frequencies could be potentially used to obtain reliable BCC measurements.

We used a mixed-effects linear model with random intercept and slope to understand lesional and normal skin conductivity and relative permittivity frequency–response trajectories. The use of multifrequency data in our modeling approach is based on the bioimpedance principle that has long recognized that single frequency data offer limited insight into tissue conditions (Grimnes and Martinsen, 2014). Our modeled results indicate the ability to detect skin electrical changes associated with BCC versus with adjacent normal skin. Histological alterations within developing BCC, including scaling, telangiectasia, fibroplasia, and other remodeling changes at the dermal–epidermal junction and in the dermis, will likely impact the flow of electrical current through the lesion, supporting the observed differences in electrical conductivity and relative permittivity intercept values. Additional subject-specific factors that will likely affect our data that were not modeled in this study include age, sex, skin hydration status, the extent of previous sun exposure and solar elastosis observed histologically, body site, skin temperature, and Fitzpatrick skin type and ethnicity. We suspect that improvements will likely be achieved by accounting for these variables in our modeling approach, which ultimately could impact the accuracy of diagnosis.

In previous impedance studies on BCC (Beetner et al., 2003; Dua et al., 2004), electrical impedance readings were arbitrarily normalized by the calculation of a ratio between different frequencies to minimize skin–electrode impedance polarization artifacts and the associated biological variations, including body site, age, and gender (Aberg et al., 2005, 2004). Although this approach has shown clinical value for disease classification purposes, it has an

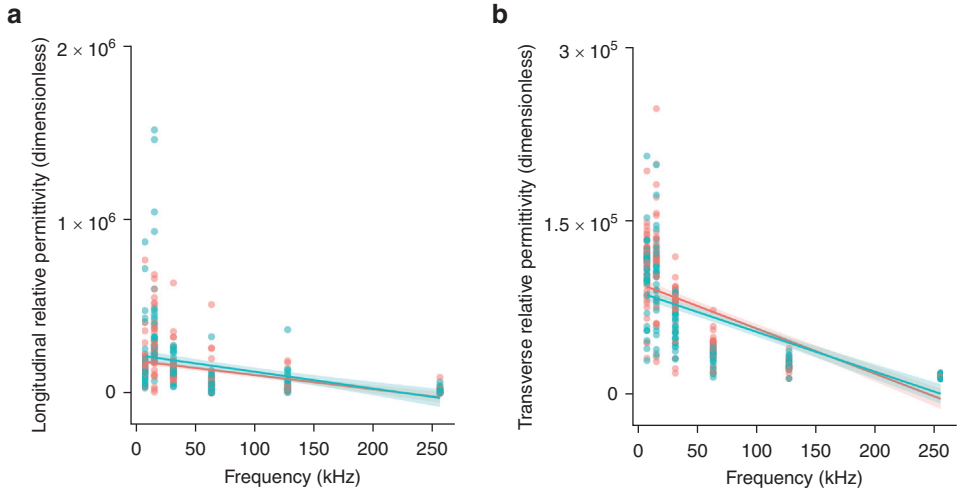

Figure 3. The relative permittivity of BCC and normal adjacent skin. BCC (red) and nonlesional adjacent skin (blue) dots represent individual relative permittivity values obtained in (**a**) longitudinal and (**b**) transverse directions, including all repeated measurements and subjects. The solid lines are the modeled trajectories, including 95% confidence intervals. BCC, basal cell carcinoma.

Table 3. Summary of Modeled Conductivity and Relative Permittivity Differences

	Longitudinal Conductivity			Transverse Conductivity			Longitudinal Relative Permittivity			Transverse Relative Permittivity		
Predictors	**Estimates**	**CI (95%)**	***P*-Value**	**Estimates**	**CI (95%)**	***P*-Value**	**Estimates**	**CI (95%)**	***P*-Value**	**Estimates**	**CI (95%)**	***P*-Value**
Intercept	129.84E−3	100.67E−3–159.01E−3	<0.001	59.35E−3	52.17E−3–66.53E−3	<0.001	203,742.03	180,292.58–227,191.49	<0.001	86,895.27	81,554.25–92,236.29	<0.001
Frequency	1.5E−3	1.25E−3–1.74E−3	<0.001	0.25E−3	0.21E−3–0.30E−3	<0.001	−892.74	−1,055.21 to −730.28	<0.001	−401.59	−441.78 to −361.41	<0.001

Abbreviations: CI, confidence interval.

Estimates, 95% CIs, and statistical significance *P*-values were obtained, analyzing multifrequency values using a linear mixed-effects model for each dataset with random intercept and slope terms.

important caveat: disentangling the underlying physiological source(s) from ratiometric impedance values represents a technical complexity yet to overcome. For example, Birgersson et al. (2013) attempted to remove skin–electrode impedance polarization artifacts affecting SciBase II, but limitations associated with the approach resulted in large (up to 75%) skin VCP errors reported by the authors. As part of our impedance research efforts, we built a four-electrode EID device robust to skin–electrode polarization errors and thus capable of measuring accurately the VCPs of tissues and tested it in measurements on the tongue (Luo et al., 2021). The associated cost to obtain this information is an increase in measurement complexity because it required at least 12 electrodes to measure in at least three different directions (3 directions × 4 electrodes/direction) (Luo and Sanchez, 2021). In this study, we made changes to our system specifically for skin measurements, including building a 16-electrode array, in total, 16 electrodes to measure in four different directions to have redundant data (4 directions × 4 electrodes/direction). Despite the increased complexity, the process of obtaining the VCPs of the skin with URSKIN is fully automated, is transparent to the operator, and required <1 minute to complete one skin measurement.

Although URSKIN shows promise to improve cancer screening efficiency, further research is needed to assess its sensitivity and specificity for BCC diagnosis. The device is also limited in the number of frequencies and frequency range that it can measure; it may be possible to improve the sensitivity to detect alterations by increasing the number of frequencies and the frequency range measured as well as using an array of silicon nanoneedles or microneedles for penetrating the stratum corneum layer. However, these electrodes are not easy or cheap to manufacture and typically require access to a specialized silicon manufacturing facility. The design of the device must also balance minimizing invasiveness and maximizing reliability with durability and capability to completely penetrate the stratum corneum. Comparatively, widely available printed circuit manufacturing processes used in this study provide a cost-efficient alternative, making it relatively easy to make changes with a short lead time.

Additional computer simulations were performed to quantify the depth of skin measured with URSKIN; this information cannot be obtained through any other method. The simulation results indicate that the volume of tissue measured underneath the electrodes has dimensions of length 13 mm × width 17 mm × depth 7 mm (Figure 4). No differences in depth were observed between simulations changing the electrical current at the frequencies measured from 8 to 256 kHz. This depth sensitivity could be used to target the epidermis, papillary dermis, or reticular dermis simply by changing the spacing and arrangement of the electrodes. We foresee a future clinical translation of selective or spatial targeting to aid in distinguishing superficial BCC from micronodular or infiltrative subtypes or in determining the subclinical extension of disease to guide therapy.

There are several limitations of this study. First, we intentionally did not address diagnostic differences between subjects with BCC and healthy volunteers or compare skin VCPs with histological data, although all patients had histology

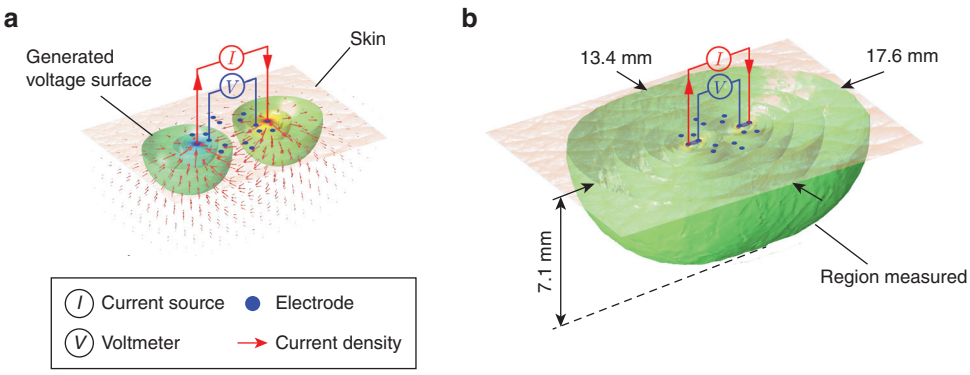

Figure 4. EID simulation. (**a**) Qualitative FEM simulation at 8 kHz shows the distribution of electrical current through the skin model and the voltage surfaces generated within the tissue during an EID measurement. (**b**) Quantitative FEM analysis to assess the region of tissue and depth underlying the electrodes measured with URSKIN. EID, electrical impedance dermography; FEM, finite element model.

performed as part of the study. Second, the technology employed was a custom-built prototype. For example, expanding the number of frequencies, the frequency range, and the positioning of the current electrodes further from the voltage-measuring electrodes would expect to allow us to fully characterize the VCPs of BCC and improve the sensitivity to detect even deeper skin lesions. Third, we modeled the VCPs of the skin. Whereas previous work has shown that various nonstandardized relative impedance-derived metrics (e.g., arbitrarily defined ratios of impedance values at high and low frequencies) allow for BCC classification (Emtestam et al., 1998), values of electrical conductivity and relative permittivity in BCC reported in this study are, by definition, absolute (not relative) and standard. Clearly, the results will require further validation in future studies to evaluate different histologic subtypes of BCC, which we plan on pursuing as a logical next step to this work. Fourth, as a single-site investigation, it will be important to replicate these findings in a multicenter cohort. Fifth, we have only examined a mixed-effects linear model in our outcomes. We are currently using machine-learning approaches to obtain a more accurate representation of frequency trajectories, including subject-specific information, and also to diagnose skin lesions. However, we are restricted from doing so in this study by the limited sample size in this pilot study.

Despite these limitations, we have shown that URSKIN provides a quick, convenient, reproducible means for performing EID of BCC and nonlesional adjacent skin in the clinic. Our approach is noninvasive and provides objective, quantitative, and standardized data reflecting the electrical status of the skin; its ease of use requires minimal operator training; and none of the subjects reported discomfort during the measurements. These early results suggest that our URSKIN is a promising biomarker for performing rapid and reliable skin lesion profiling in the clinical setting. Future studies generating normative lesional data, assessing the differences in electrical signature in other skin conditions, evaluating the utility in diagnosing skin cancer using machine-learning approaches, and comparing skin electrical data with clinically accepted outcomes are planned.

MATERIALS AND METHODS

Study subjects

This study was approved by the Institutional Review Board at the University of Utah, and all participants gave previous written informed consent. Our technology received Institutional Review Board approval for human testing as a nonsignificant risk investigational device. A total of 18 patients were studied. The inclusion criteria were age ≥18 years with a lesion clinically suspicious for BCC of at least 5 mm in diameter that was to be biopsied. Subjects with lesions on the face, haired scalp, or genital area were excluded.

Experimental protocol

Figure 1 shows the device used in this study as well as the dimensions and details on the electrodes' disposition. The electrodes were sterilized with 70% isopropyl alcohol before each measurement. After informed written consent was obtained, any hairs around the lesion were removed using small scissors, and the skin region was cleaned using disposable gauze moistened with sterile saline. After 10 seconds, the electrode array was positioned against the skin, applying gentle pressure to ensure good electrical contact. The operator then performed a measurement. The procedure was repeated at least two more times by the same operator to provide a minimum of three measurements. The device was taken off the skin in between repeated measurements and then positioned again. At the completion of the lesional measurements, a fresh piece of gauze was used to clean nearby normal skin at 2 inches from the lesion, and the sequence was repeated so that three or more control measurements were obtained. All measurements were obtained in approximately 5 minutes. As a part of standard of care, a shave biopsy of the suspicious lesion was then performed and sent for routine processing and histologic analysis. The results of the biopsy but not of the EID measurements were made available to the subjects.

Device

URSKIN is a portable handheld EID device to measure the skin at the clinic. The device is powered by a battery and communicates with a custom smartphone application through Bluetooth (please see Supplementary Materials and Supplementary Figure S1 for further details regarding the use of the application). The device automatically applies a painless, safe, alternating electrical current starting at 8, 16, 32, 64, 128, and 256 kHz in four different directions sequentially as determined by the angles 0, 45, 90, and 150 degrees. To perform a measurement, the device automatically sweeps both the frequency of electrical current and the measuring direction sequentially. For each measuring direction (Figure 5), the device applies an electrical current through outer ring current electrodes in that direction only (shown in red) and then measures the generated voltage through the inner voltage electrodes in that direction only (shown in blue).

The red arrow in Figure 5 is the electrical symbol for a current generator, and the direction of the arrow indicates the direction of

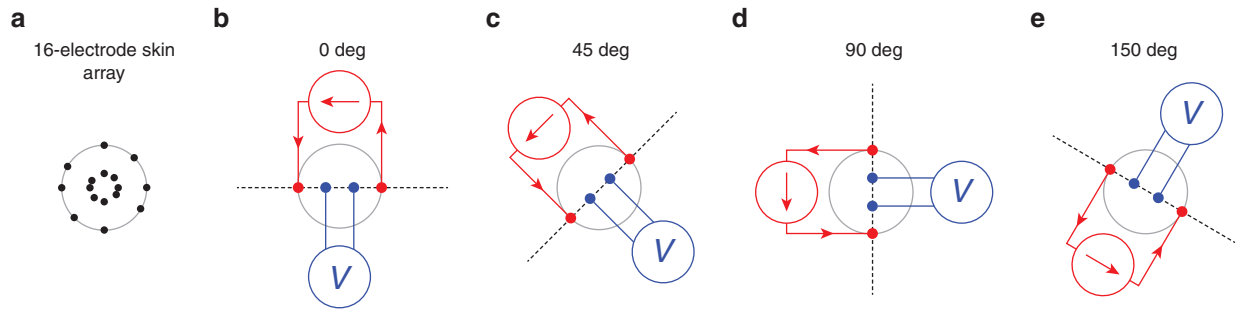

Figure 5. Electrical connections to perform an EID measurement. (**a**) Schematic illustrating a plane view of the 16-electrode array. Electrical connection of the current generator and voltmeter to the outer current (in red) and inner voltage (in blue) electrodes measuring in four directions: (**b**) 0, (**c**) 45, **(d)**, 90, **(e)** 150 deg. deg, degree; EID, electrical impedance dermography.

the current flow through the skin. As shown in Figure 5, the current generator applies alternating electrical current between the outer current electrodes. One of the current electrodes injects current into the skin, while at the same time, the opposite current electrode drains from the skin the current needed to close the electrical circuit. At the same time, the inner voltage electrodes in that particular direction measure the generated electrical voltage. By measuring the difference between voltage electrodes using a voltmeter circuit and knowing the electrical current applied, the device calculates the skin impedance using Ohm's law: impedance equals voltage divided by current. During a measurement, the current and voltage electrodes in different directions from those colored in Figure 5b (i.e., electrodes shown in Figure 5c–e), Figure 5c (i.e., electrodes shown in Figure 5b, d, and e), Figure 5d (i.e., electrodes shown in Figure 5b, c, and e), and Figure 5e (i.e., electrodes shown in Figure 5b–d) are not connected to the current generator or the voltmeter and therefore were not used.

Once the skin impedance data are measured in all the four directions and frequencies, the device informs the operator through the smartphone application. At this point, the operator can remove the device from the skin because the measurement is completed. At the same, the device automatically proceeds to process the data; this takes a few seconds only. Skin impedance data measured in all the four directions at one specific frequency are processed by the device sequentially to calculate the skin conductivity and relative permittivity in longitudinal and transverse directions at that frequency in particular. Once the calculation is completed, the device proceeds to calculate the VCPs at the next frequency measured until all the six measurement frequencies are analyzed. The results of these calculations are 24 different datasets: 2 (conductivity and relative permittivity) × 2 (longitudinal and transverse directions) × 6 (8, 16, 32, 64, 128, and 256 kHz). Next, the device transfers these data through Bluetooth to the application. On completion, the application notified the Operator and so that she/he can proceed to plot the data in the smartphone application to verify the values and perform a new measurement. Deidentified data are automatically stored in the phone, and also they can be sent from the application itself easily by e-mail just by tapping the Send data button.

Electrode array

The skin electrode array is a custom-designed printed circuit board manufactured by JLCPCB (Guangdong, China) (Figure 1). The printed circuit board contains a total of 16 noninvasive surface electrodes for four-electrodes measurements defined by the angles 0, 45, 90, and 150 degrees. The outer pair of electrodes spaced 4.2 mm apart apply electrical current into the skin, whereas the inner pair electrodes at a distance of 2.8 mm apart measure the generated voltage signal.

Finite element model simulations

Finite element model simulations were performed in the frequency domain using AC/DC Module, Electric Currents Physics in Comsol Multiphysics software, version 5.2 (Comsol, Burlington, MA). To determine the depth of measurement using URSKIN, we created a finite element model rectangular slab mimicking a large portion of skin with dimensions 10 times larger than the electrodes' maximum distance as shown in Figure 1. The spatial dependence of the skin conductivity and relative permittivity properties were averaged from our clinically normal measurements. The finite element model was then broken down into small elements (a process termed discretization or meshing), from which to calculate individual element current and voltages shown in Figure 4. This computational process is necessary to quantitatively evaluate the depth of measurement through a numerical sensitivity analysis. This sensitivity analysis consists of quantifying the percentage contribution of each discretized element from the model to the impedance measured by the surface electrodes. The sensitivity region shown in Figure 4 reflects the overall expected skin volume measured with URSKIN contributing 99% of a total of 100% to the measured data. In other words, cancer-induced electrical changes outside this colored sensitivity region are expected to contribute <1% to the recordings, and they would probably be undetected with the simulated electrode configuration.

Data analysis

Skin conductivity and relative permittivity data were analyzed using R software (R Foundation for Statistical Computing, Vienna, Austria). Standard ICCs were calculated to describe how strongly repeated measurements resembled each other. ICCs are typically used to determine the technique's intrasession reproducibility as well as its 95% confidence intervals. Multifrequency-paired analysis was performed using a linear mixed-effects model for each dataset with random intercept and slope terms to account for within-subject correlations and between-subject variability. For these analyses, the main parameter of interest was the intercept difference because it has the most direct relevance to skin physiology.

Data availability statement

Datasets related to this article can be found at the Sanchez Research Lab website at the University of Utah (https://srl.ece.utah.edu/publications/).

ORCIDs
Xuesong Luo: http://orcid.org/0000-0003-4142-1402
Ye Zhou: http://orcid.org/0000-0001-9367-7608
Tristan Smart: http://orcid.org/0000-0002-0690-8736
Douglas Grossman: http://orcid.org/0000-0003-1790-7023
Benjamin Sanchez: http://orcid.org/0000-0002-1594-9847

AUTHOR CONTRIBUTIONS
Conceptualization: DG, BS; Formal Analysis: YZ, BS; Investigation: TS; Methodology: XL, BS Writing - Original Draft Preparation: DG, BS; Writing - Review and Editing: XL, YZ, TS, DG, BS

ACKNOWLEDGMENTS
DG was supported by the University of Utah Department of Dermatology and the Huntsman Cancer Foundation. The authors are thankful to Elise Brunsgaard and Kenneth Boucher, co-directors of the Cancer Biostatistics Shared Resource at Huntsman Cancer Institute at the University of Utah, for their comments on the manuscript.

CONFLICT OF INTEREST
BS holds equity in Haystack Diagnostics, a company that develops clinical needle impedance technology for neuromuscular evaluation. The company has an option to license patented needle impedance technology where the author is named an inventor. He also holds equity and serves as Scientific Advisory Committee Member of Ioniq Sciences, a company that develops clinical impedance technology for early lung and breast cancer detection. BS holds equity and serves as scientific advisor to the Board of B-Secur, a company that develops impedance technology. He consults for Myolex, a company that develops surface impedance technology. The company has an option to license patented surface impedance technology where the author is named an inventor. BS also serves as a consultant to Impedimed, a company that develops clinical impedance technology for early detection of secondary lymphedema. The company has an option to license patented impedance technology where the author is named an inventor. He also serves as a consultant to Texas Instruments, Happy Health, and Maxim Integrated, companies that develop impedance-related technology for consumer use. G is an investigator for Dermtech and Orlucent, both companies developing noninvasive technologies for melanoma diagnosis, and also serves on the Advisory Board of Orlucent. The remaining authors state no conflict of interest.

SUPPLEMENTARY MATERIAL
Supplementary material is linked to the online version of the paper at www.jidonline.org, and at https://doi.org/10.1016/j.xjidi.2021.100075.

REFERENCES
Aberg P, Geladi P, Nicander I, Hansson J, Holmgren U, Ollmar S. Non-invasive and microinvasive electrical impedance spectra of skin cancer - a comparison between two techniques. Skin Res Technol 2005;11:281–6.

Aberg P, Nicander I, Hansson J, Geladi P, Holmgren U, Ollmar S. Skin cancer identification using multifrequency electrical impedance–a potential screening tool. IEEE Trans Bio Med Eng 2004;51:2097–102.

Alonso E, Giannetti R, Rodríguez-Morcillo C, Matanza J, Muñoz-Frías JD. A novel passive method for the assessment of skin-electrode contact impedance in intraoperative neurophysiological monitoring systems. Sci Rep 2020;10:2819.

Beetner DG, Kapoor S, Manjunath S, Zhou X, Stoecker WV. Differentiation among basal cell carcinoma, benign lesions, and normal skin using electric impedance. IEEE Trans Bio Med Eng 2003;50:1020–5.

Birgersson U, Birgersson E, Nicander I, Ollmar S. A methodology for extracting the electrical properties of human skin. Physiol Meas 2013;34:723–36.

Braun RP, Mangana J, Goldinger S, French L, Dummer R, Marghoob AA. Electrical impedance spectroscopy in skin cancer diagnosis. Dermatol Clin 2017;35:489–93.

Dua R, Beetner DG, Stoecker WV, Wunsch DC 2nd. Detection of basal cell carcinoma using electrical impedance and neural networks. IEEE Trans Biomed Eng 2004;51:66–71.

Emtestam L, Nicander I, Stenström M, Ollmar S. Electrical impedance of nodular basal cell carcinoma: a pilot study. Dermatology 1998;197:313–6.

Foster KR, Schwan HP. Dielectric properties of tissues and biological materials: a critical review. Crit Rev Biomed Eng 1989;17:25–104.

Geddes LA. Who introduced the tetrapolar method for measuring resistance and impedance? IEEE Eng Med Biol Mag 1996;15:133–4.

Glickman YA, Filo O, David M, Yayon A, Topaz M, Zamir B, et al. Electrical impedance scanning: a new approach to skin cancer diagnosis. Skin Res Technol 2003;9:262–8.

Grimnes S, Martinsen OG. Bioimpedance and bioelectricity basics. 3rd ed. Cambridge, MA: Academic Press; 2014.

Luo X, Gutierrez Pulido HV, Rutkove SB, Sanchez B. In vivo muscle conduction study of the tongue using a multi-electrode tongue depressor. Clin Neurophysiol 2021;132:683–7.

Luo X, Sanchez B. *In silico* muscle volume conduction study validates *in vivo* measurement of tongue volume conduction properties using a user tongue array depressor. Physiol Meas 2021;42:045009.

Malvehy J, Hauschild A, Curiel-Lewandrowski C, Mohr P, Hofmann-Wellenhof R, Motley R, et al. Clinical performance of the Nevisense system in cutaneous melanoma detection: an international, multicentre, prospective and blinded clinical trial on efficacy and safety. Br J Dermatol 2014;171:1099–107.

March J, Hand M, Grossman D. Practical application of new technologies for melanoma diagnosis: part I. Noninvasive approaches [published correction appears in J Am Acad Dermatol 2015;73:720]. J Am Acad Dermatol 2015;72:929–42.

McAdams ET, Lackermeier A, McLaughlin JA, Macken D, Jossinet J. The linear and non-linear electrical properties of the electrode-electrolyte interface. Biosens Bioelectron 1995;10:67–74.

Rocha L, Menzies SW, Lo S, Avramidis M, Khoury R, Jackett L, et al. Analysis of an electrical impedance spectroscopy system in short-term digital dermoscopy imaging of melanocytic lesions. Br J Dermatol 2017;177:1432–8.

Sanchez B, Martinsen OG, Freeborn TJ, Furse CM. Electrical impedance myography: a critical review and outlook. Clin Neurophysiol 2021;132:338–44.

Schwan HP. Electrical and acoustic properties of biological materials and biomedical applications. IEEE Trans Biomed Eng 1984;31:872–8.

Schwan HP. Linear and nonlinear electrode polarization and biological materials. Ann Biomed Eng 1992;20:269–88.

Stephens WGS. The current-voltage relationship in human skin. Med Electron Biol Engng 1963;1:389–99.

Yamamoto T, Yamamoto Y. Electrical properties of the epidermal stratum corneum. Med Biol Eng 1976;14:151–8.

SUPPLEMENTARY MATERIALS AND METHODS

Smartphone application

The device is controlled by Bluetooth through the application (Supplementary Figure S1). First, the operator must enter the operator and patient identifiers (Supplementary Figure S1a and b). After turning on the device, the operator then needs to pair it to the smartphone through Bluetooth (Supplementary Figure S1c). Next, the operator is instructed to place the electrodes above the skin region of interest (Supplementary Figure S1d). Once the measurement is started, a percentage is displayed to inform the operator of the approximate time remaining to finish the measurement (Supplementary Figure S1e). Once the measurement is finished, the operator is informed to remove the electrodes, and the data are immediately processed and transferred from the device to the application (Supplementary Figure S1f). The operator can then view the data in real-time in the application (Supplementary Figure S1g and h) after completing a measurement. The operator can then repeat the measurement and/or send deidentified data by e-mail (Supplementary Figure S1i). In the end, the operator must quit the application before measuring the next participant and repeat the same steps (Supplementary Figure S1j).

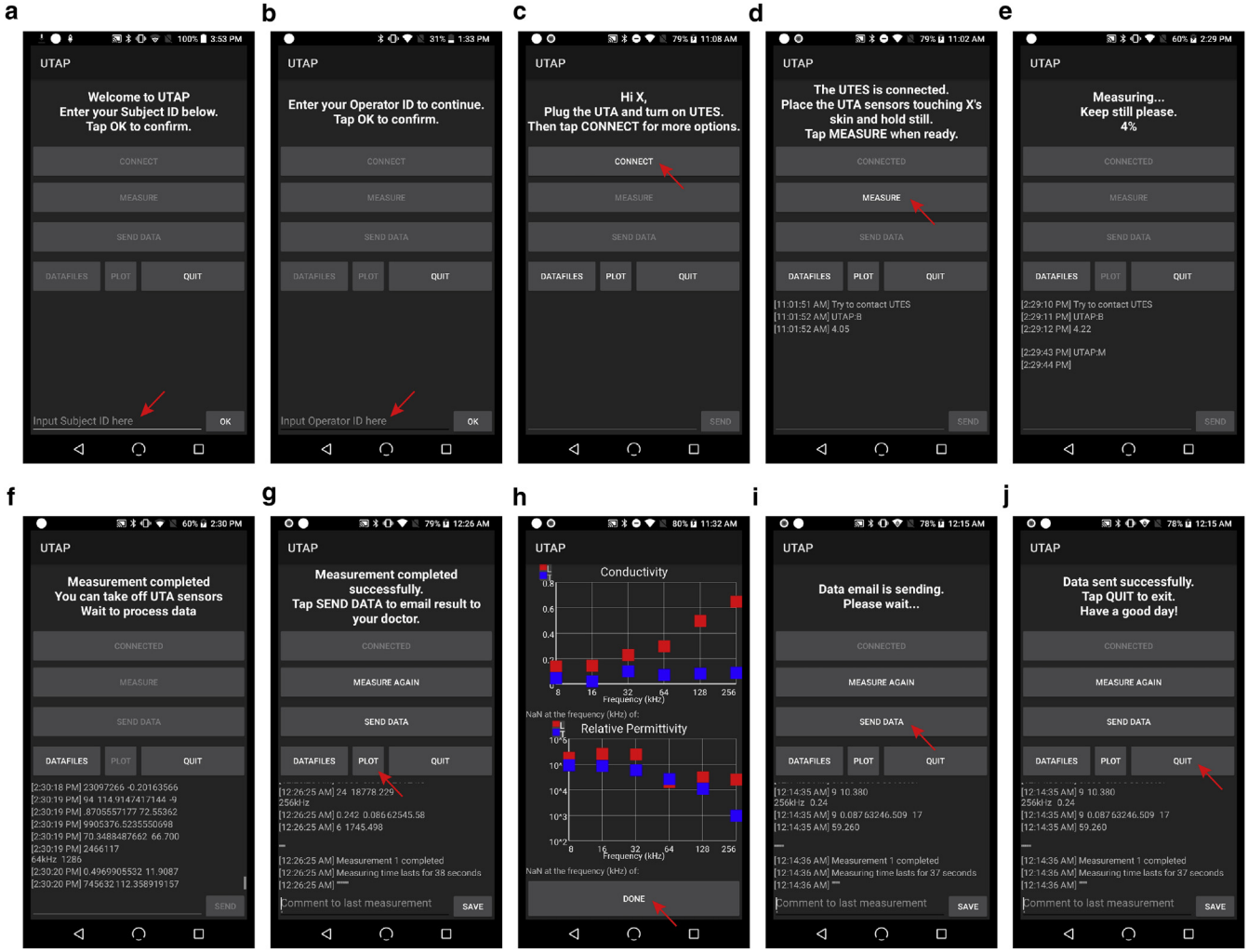

Supplementary Figure S1. Application–user interface. The application guides the operator from step **a** to **j** to complete measurement and e-mail the data for further analysis.